Seismic evaluation of self-centering steel frames using post-tensioned connections with web energy dissipation devices

Conference Paper · July 2013

CITATIONS
0

READS
88

4 authors:

Athanasios I. Dimopoulos
The University of Warwick
5 PUBLICATIONS **93** CITATIONS
SEE PROFILE

Vasileios Kamperidis
Abertay University
6 PUBLICATIONS **11** CITATIONS
SEE PROFILE

Theodore L. Karavasilis
University of Patras
93 PUBLICATIONS **1,224** CITATIONS
SEE PROFILE

G. Vasdravellis
Heriot-Watt University
48 PUBLICATIONS **447** CITATIONS
SEE PROFILE

SECED - Society for Earthquake and Civil Engineering Dynamics
Young Engineers Conference - 2013

Seismic evaluation of self-centering steel frames using post-tensioned connections with web energy dissipation devices

A.I. Dimopoulos[1], V.C. Kamperidis[1], T.L. Karavasilis[1], G. Vasdravellis[2]

[1] *School of Engineering, University of Warwick, Coventry, United Kingdom*
[2] *School of the Built Environment, Herriot Watt University, Edinburgh, United Kingdom*
Email: T.Karavasilis@warwick.ac.uk

ABSTRACT

A new self-centering steel post-tensioned connection using web hourglass shape steel pins (WHPs) has been recently developed and experimentally validated. The connection isolates inelastic deformations in WHPs and avoids damage in other connection parts, like beams and columns. WHPs do not interfere with the composite slab and can be very easily replaced without bolting or welding, and so, the connection enables rapid return to building occupancy in the aftermath of a strong earthquake. This paper presents a simplified nonlinear model for the connection that consists of nonlinear beam-column elements, and hysteretic and contact spring elements appropriately placed in the beam-column interface. The model was calibrated against experimental results and found to accurately simulate the connection behaviour. A prototype building was selected and designed both as a conventional steel moment-resisting frame (MRF) and as a self-centering steel MRF (SC-MRF) using the proposed connection. Seismic analyses show that both MRF and the SC-MRF have comparable storey drifts, and highlight the ability of the SC-MRF to eliminate damage in beams and residual drifts. The paper also shows that damage repair for the MRF will be costly and disruptive after the design basis earthquake, and, not financially viable after the maximum considered earthquake.

1. INTRODUCTION

Conventional ductile steel moment-resisting frames (MRFs) are currently designed to form a global plastic mechanism under strong earthquakes by developing plastic hinges at the ends of the beams and at the base of the columns (EC8 2004). This design approach results in softening force-drift behaviour, and so, has many advantages including reduced member forces and low base shear force. However, plastic hinges in structural members involve cyclic inelastic deformations and local buckling which result in difficult to inspect and repair damage as well as residual drifts. The socio-economic losses related to damage and residual drifts are repair costs, loss of building occupation and business interruption, and possibly building demolition due to the complications associated with repairing large residual drifts (Mc Cormick et al., 2008).

A new steel post tensioned (PT) connection using web hourglass shape steel pins (WHPs) has been recently developed and validated both experimentally and with finite elements analysis (Vasdravellis et al., 2012, 2013). The connection isolates inelastic deformations in WHPs, avoids damage in other connection parts as well as in beams and columns, and, eliminates residual drifts. WHPs do not interfere with the composite slab and are very easy-to-replace without bolting or welding, and so, the connection enables non-disruptive repair and rapid return to building occupancy in the aftermath of a strong earthquake. In this paper a simplified nonlinear model for the PT connection with WHPs that consists of nonlinear beam-column elements, hysteretic and contact spring elements appropriately placed in the beam-column interface is presented. The model was calibrated against experimental results and found to accurately simulate the connection behaviour. A prototype building was selected and designed both as conventional steel MRF and as steel SC-MRF using PT connections with WHPs. The design process, proposed by (Vasdravellis et al., 2012) resulted in the same beam and column cross sections for the conventional MRF and the SC-MRF, while WHPs and the required beam flange reinforcing plates of the SC-MRF have practical sizes. Nonlinear models for the conventional MRF and the SC-MRF were developed in OpenSees (Mazzoni et al., 2006) and used to conduct seismic analyses that show that the conventional MRF and the SC-MRF have comparable peak storey drifts. The SC-MRF eliminates damage in beams and residual drifts, and so, avoids disruptive repair after the design basis earthquake (DBE) and the maximum considered earthquake (MCE). On the other hand, repair of damage in the conventional MRF will be costly and disruptive after the DBE, and, not financially viable after the MCE due to large residual drifts.

2 STEEL POST-TENSIONED CONNECTION WITH WHPs

Fig. 1.a shows a schematic representation of a SC-MRF incorporating PT connections with WHPs and the details of an exterior PT connection (Fig. 1.b). Two high strength steel bars located at the mid-depth of the beam, one at each side of the web, pass through holes drilled on the column flanges. The bars are post-tensioned and anchored to the exterior column flange, and so, clamp the beam to the column. Four WHPs are inserted in aligned holes drilled on the web of the beam and on strong supporting plates. The supporting plates are welded on the column flanges and have large thickness to provide fixed support boundary conditions to WHPs. Energy dissipation is provided by inelastic bending of the WHPs which are symmetrically placed (close to the top and bottom beam flange) to provide increased lever arm, and so, increased internal moment resistance. WHPs are designed to have an hourglass shape to provide enhanced energy dissipation and fracture capacity (Kobori et al., 1992) as shown in Fig. 1.c Both sides of the beam web are reinforced with steel plates to increase the contact surface of the WHPs with the web. In that way, possible ovalization of the holes drilled on the web and the reinforcing plates under the WHP bearing forces will be negligible and pronounced pinching behavior under cyclic deformations can be avoided. The connection includes beam flange reinforcing plates to avoid excessive early yielding in the beam flanges under the high PT bars forces. In addition, the panel zone is strengthened with doubler and continuity plates.

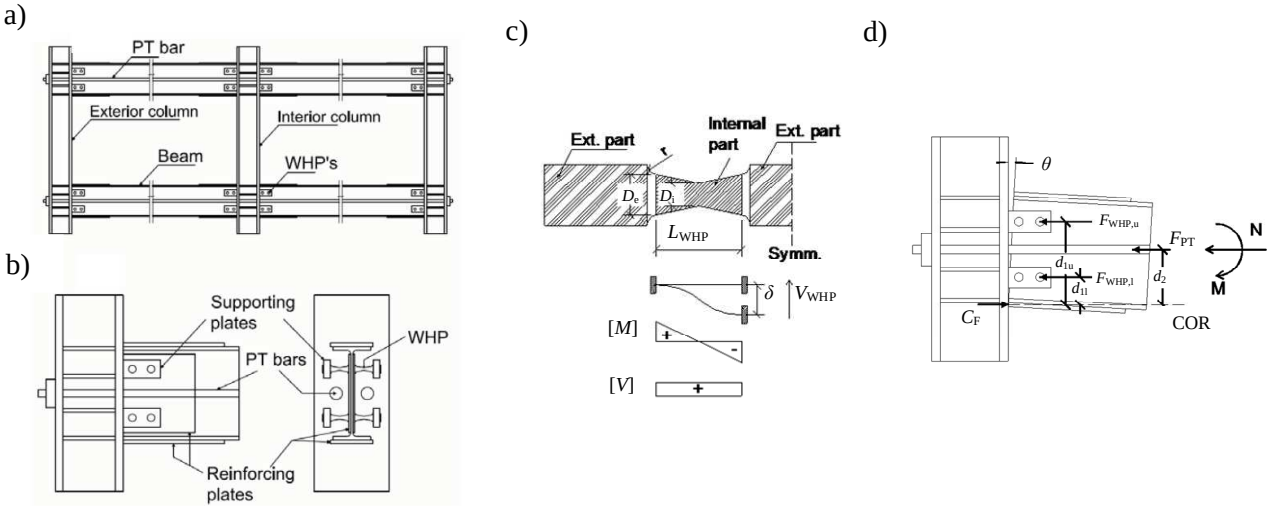

Figure 1 (a) SC-MRF incorporating PT connections with WHPs; (b) exterior PT connection details; (c) Geometry of half a WHP; (d) Gap opening mechanism

The connection behavior is characterized by gap opening and closing in the beam-column interface as a result of the re-centering force in the PT bars. Fig. 1.d shows the gap opening mechanism in the connection where d_{1u} and d_{1l} are the distances of the upper and lower WHPs from the center of rotation (COR), respectively; d_2 is the distance of the PT bars from the COR; F_{PT} is the total force in both PT bars; $F_{WHP,u}$ and $F_{WHP,l}$ are the forces in the upper and lower WHPs, respectively; and CF is the compressive force on the beam-column bearing surface. It is assumed that the COR is located at the inner edge of the beam flange reinforcing plate. This assumption has been verified by the large-scale experiments previously conducted by (Vasdravellis et al., 2012). A design procedure for the proposed PT connection with WHPs has been developed by (Vasdravellis et al., 2012) and validated in steel frames by (Dimopoulos et al., 2012).

3 MODELING OF PT CONNECTION WITH WHPs FOR NONLINEAR ANALYSIS

A model for the PT connection with WHPs and the associated beams and columns was developed in OpenSees as shown in Fig. 2.a. The beams and columns were modeled using the nonlinear force-based beam-column fiber element. For the beam, two fiber elements with cross-sections having different flange thickness were used to account for the beam flange reinforcing plates. Each fiber was associated with uniaxial bilinear elastoplastic stress-strain behaviour (Steel01 in OpenSees) with a post-yield stiffness ratio equal to 0.01.

Rigid elastic beam-column elements were used to model the beam-column interface where gap opening and

closing takes place. To accurately capture the gap opening mechanism in the beam-column interface, three zero-length contact spring elements were placed at equal spaces along the beam flange thickness. These contact springs were associated with an elastic compression - no tension force-displacement behaviour (ENT material in Openness). A value of the compression stiffness equal to 20 times the axial stiffness of the beam K_b was assigned to these contact springs. To capture the hysteretic energy dissipation capacity of the connection, two zero-length hysteretic springs were placed at the exact locations of WHPs along the depth of the beam web. These springs were associated with a smooth hysteretic Giuffre-Menegotto-Pinto model with isotropic hardening (Steel 02 material in OpenSees). Specific properties of the Steel 02 material are given in the work of (Dimopoulos et al., 2012) in order to capture the accurate behavior of the WHPs.

To account for panel zone shear deformations and possible yielding, the panel zone was modeled using the Scissors model which introduces four additional rigid elastic beam-column elements and two nodes in the center of the panel zone connected with two zero-length rotational springs. These springs are associated with bilinear elastoplastic hysteretic rules (Steel01 material in OpenSees) with properties calculated to reflect the contribution of the column web (including doupler plates) and the column flanges in the shear force - shear deformation panel zone behaviour. This simple panel zone model has been found to produce identical results to those of the more computationally expensive Krawinkler panel zone model (Charney and Downs, 2004).

PT bars were modeled using a truss element running parallel to beam center-line axis and connected to the exterior nodes of the panel zones of the exterior columns of the SC-MRF. The truss element has a cross-section area A_{PT} equal to that of both PT bars. To account for post-tensioning, an initial strain equal to $F_{PT,\,i}/(A_{PT} \cdot E_{PT})$ was first assigned to the truss element where E_{PT} is the modulus of elasticity of the PT bar material. However, post-tensioning results in shortening of the beams which in turn decreases the post-tensioning force. To account for this decrease, the initial strain in the truss element was increased to ensure that the post-tensioning force in the PT bars will be equal to $F_{PT,\,i}$ after the beam shortening. The accuracy of the model for the PT connection with WHPs and the associated beams and columns was assessed using results from large-scale experimental tests previously conducted by (Vasdravellis et al., 2012). Fig. 2.b shows the experimental test setup and Fig. 2.c shows the experimental and analytical hysteresis for the PT connection and confirms a good agreement between the proposed model and the test results.

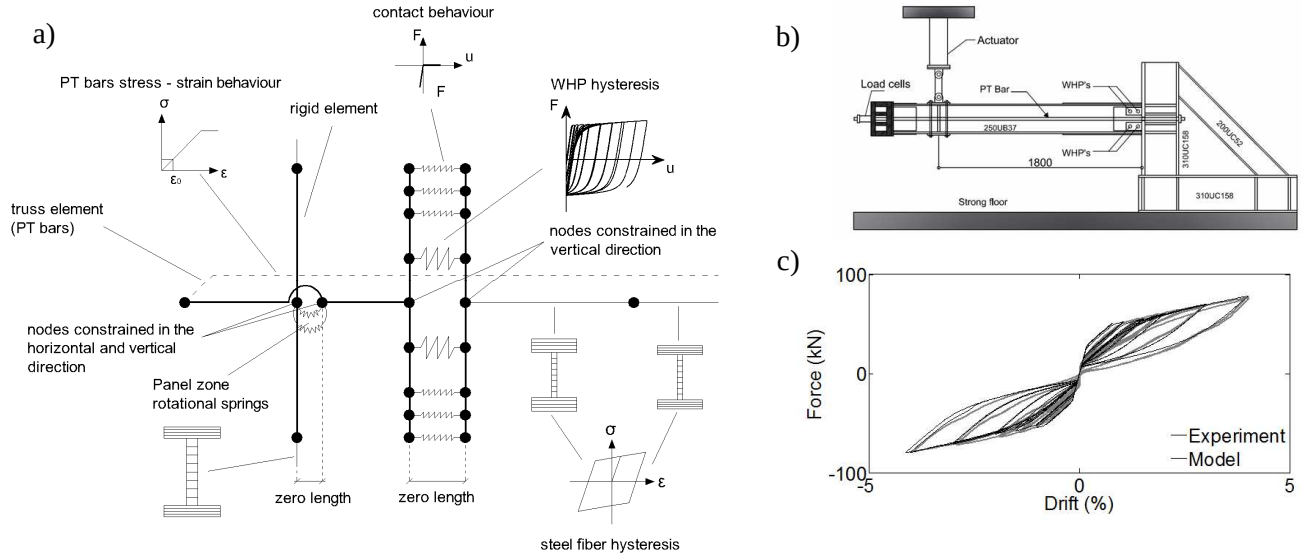

Figure 2 (a) Assumed cyclic behavior of a PT connection with WHPs; (b) Setup for PT connection cyclic tests; (c) comparison of experimental hysteresis and hysteretic model

4 PROTOTYPE BUILDING – DESIGN OF MRF AND SC-MRF

Fig. 3.a shows the plan view of the 5-storey, 4-bay by 3-bay prototype office building used for the study. The building has four identical frames to resist lateral loads in the longitudinal plan direction. The design study focused on one of the interior frame shown in Fig. 3.b, which was designed either as a conventional steel MRF or as a steel

SC-MRF using PT connection with WHPs to compare their seismic performance. The design seismic action expressed by the Type 1 elastic response spectrum of EC8 with peak ground acceleration equal to 0.30g and ground type B. The MRF was designed according to EC3 and EC8. The steel yield strength for columns is assumed equal to 350 MPa and for beams equal to 300 MPa. The final sections were found iteratively by decreasing the value of the behavior factor (q), designing the MRF for increased strength under the DBE and then checking storey drifts under the FOE. The fundamental period of vibration is 1.08 s. and the estimated peak storey drift $\theta_{s\text{-}max}$ is 0.64% under the FOE, 1.6% under DBE and 2.4% under the MCE. The sections of the conventional MRF were used for designing the SC-MRF so that both frames would have almost the same initial stiffness and fundamental period of vibration. The PT connections with WHPs were designed using the methodology presented in (Vasdravellis et at. 2012). Table 1 lists the column cross-sections, beam cross-sections, $F_{PT,i}$, PT bar diameter d_{PT}, D_e, D_i, L_{WHP}, and length L_{RP} and thickness t_{RP} of the beam flange reinforcing plates. The beam flange reinforcing plates are made of steel with yield strength equal to 300 MPa. The WHPs are made of steel with yield strength equal to 235 MPa. The material of the PT bars has nominal yield strength equal to 930 MPa and elongation capacity 6%. The fundamental period of vibration of the SC-MRF is 1.01 sec., i.e., slightly lower than that of the conventional MRF (1.08 sec) because the beam flange reinforcing plates increase the stiffness of the beams of the SC-MRF.

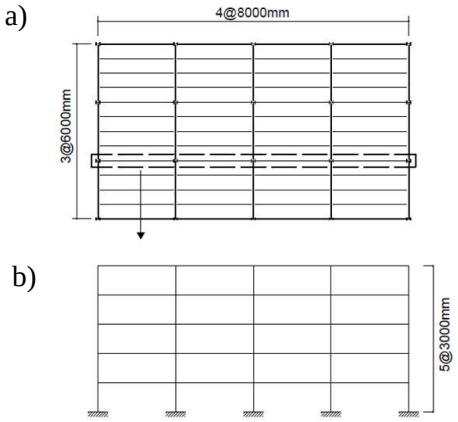

Figure 3: (a) Plan view of prototype building; (b) elevation of interior MRF

Table 1: Design details of the conventional steel MRF and the steel SC-MRF using PT connections with WHPs

Storey	Cross sections MRF & SC-MRF		PT bars		WHPs			Reinf. Plates	
	Beams	Columns	$F_{PT,I}$ (kN)	d_{PT} (mm)	D_e (mm)	D_i (mm)	L_{WHP} (mm)	L_{RP} (mm)	t_{RP} (mm)
1	IPE450	HEB400	933	36	36	26	65	1080	15
2	IPE450	HEB400	933	36	36	26	65	1080	15
3	IPE400	HEB400	806	36	33	23	65	1180	15
4	IPE400	HEB360	806	36	33	23	65	1180	15
5	IPE360	HEB360	700	36	32	22	65	1190	15

5 NONLINEAR MONOTONIC AND CYCLIC STATIC ANALYSIS

Fig. 4.a shows the base shear coefficient (V/W) - roof drift (θ_r) behaviour of the conventional MRF and the SC-MRF from nonlinear monotonic (pushover) static analysis using non-linear models described in Section3. V is the base shear and W is the seismic weight. An inverted triangular force distribution along with roof displacement control was used in these analyses. The MRF and the SC-MRF have comparable base shear strengths and comparable initial stiffness. The pushover curves are plotted along with points associated with structural limit states and vertical lines corresponding to roof drifts expected under the FOE, DBE and MCE. The structural limit states for the conventional MRF are beam yielding and base column yielding and occur at θ_r equal to 0.82% and 0.92% respectively. The conventional MRF avoids damage under the FOE but experiences significant damage under the DBE. The structural limit states for the SC-MRF are decompression in a PT connection (i.e. point 1 in Fig. 5.a), WHP yielding (i.e. point 2 in Fig. 5.a), base column yielding and beam yielding. Fig. 4.a shows that the beams of the SC-MRF are damage-free for θ_r equal or lower than 3%, i.e., drifts higher than the MCE. Damage in the SC-MRF is experienced at the column bases that yield at θ_r equal to 0.97%. No PT bar yielding is observed. The first decompression occurs at θ_r equal to 0.4% while WHPs yield at θ_r equal to 0.62% which is almost equal to the FOE drift. Decompression does not involve damage while yielding of the WHPs is acceptable under low drifts since WHPs can be easily replaced without bolting or welding. The conventional MRF experiences softening at θ_r equal to 1.25% while the SC-MRF shows a more gradual softening behaviour. In particular, the SC-MRF shows softening due to decompression in the PT connections at low drifts and further softening due to plastic deformations at the column bases and yielding of a large number of WHPs at θ_r equal to 1%. Fig. 4.b shows the V/W - θ_r behaviour of the MRF and the SC-MRF from nonlinear cyclic (push-pull) static analysis. The first cycle of the analysis is performed up to the DBE drift while the

next, up to the MCE one. The SC-MRF shows full re-centering capability under the DBE, adequate energy dissipation and a small residual drift under the MCE due to plastic deformations at the column bases. The conventional MRF shows large energy dissipation capacity due to plastic deformations at the beam ends and at the column bases, and the possibility of experiencing large residual drifts under the DBE and MCE.

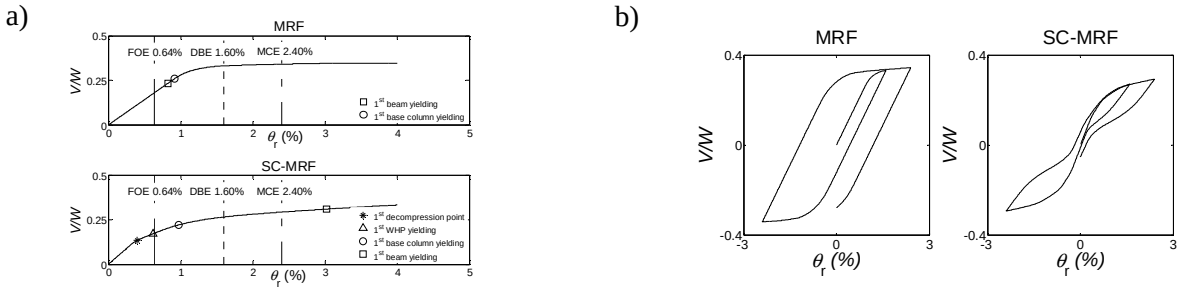

Figure 4 (a) Base shear coefficient - roof drift behaviour from nonlinear monotonic (pushover) static analysis; (b) Base shear coefficient - roof drift behaviour from nonlinear cyclic (push-pull) static analysis

6 NONLINEAR DYNAMIC TIME HISTORY ANALYSES

A set of 20 earthquake ground motions recorded on ground type B and presented in (Dimopoulos et al. 2012) without near fault directivity effects were scaled to the BDE level and used in 2D nonlinear dynamic time history analyses to evaluate the performance of the SC-MRF and the conventional MRF. The amplitudes of the DBE ground motions were further scaled by 0.4 and 1.5 to represent FOE and MCE ground motions. 2D nonlinear analytical models of the conventional MRF and the SC-MRF were developed for nonlinear dynamic analyses in OpenSees. The Newmark method with constant acceleration was used to integrate the equations of motion. The integration time step was selected to be 10 times smaller than the input time step of the earthquake ground motions. The Newton method with tangent stiffness was used to minimize the unbalanced forces within each integration time step of the nonlinear dynamic analysis. A Rayleigh damping matrix was used to model the inherent 3% critical damping at the first two modes of vibration.

Fig. 5.a shows μ, μ + σ and median $\theta_{s\text{-}max}$ values under the earthquake ground motions used in the current study scaled to the FOE, DBE and MCE. The MRF has the largest $\theta_{s\text{-}max}$ in the fourth storey with μ values equal to 0.75% under the FOE, 1.65% under the DBE and 2.2% under the MCE, i.e., close to the design values of 0.64% under the FOE and 1.6% under the DBE, and, smaller than the design value of 2.4% under the MCE. The SC-MRF has the largest $\theta_{s\text{-}max}$ in the fourth storey with mean values equal to 0.75% under the FOE, 1.8% under the DBE and 2.5% under the MCE, i.e., slightly larger than the DBE and MCE design ones. Fig. 5.b shows μ, μ + σ and median values of the residual storey drifts, $\theta_{s\text{-}res}$. $\theta_{s\text{-}res}$ show a uniform height-wise distribution for the conventional MRF and large dispersion compared to that of $\theta_{s\text{-}max}$. The largest $\theta_{s\text{-}res}$ of the conventional MRF occur in the first storey with mean values equal to 0.1% under the DBE and 0.3% under the MCE. The associated μ + σ $\theta_{s\text{-}res}$ values are equal to 0.25% under the DBE and 0.6% under the MCE. The latter $\theta_{s\text{-}res}$ values indicate that repair of damage in the conventional MRF would be costly and disruptive after the DBE and not financially viable after the MCE (Mc Cormick et al. 2008). The SC-MRF practically eliminates residual storey drifts apart from the first storey that has μ and μ + σ $\theta_{s\text{-}res}$ values equal to 0.1% and 0.15% under both the DBE and MCE. It can be assumed that there will be no need for these residual drifts to be straightened out.

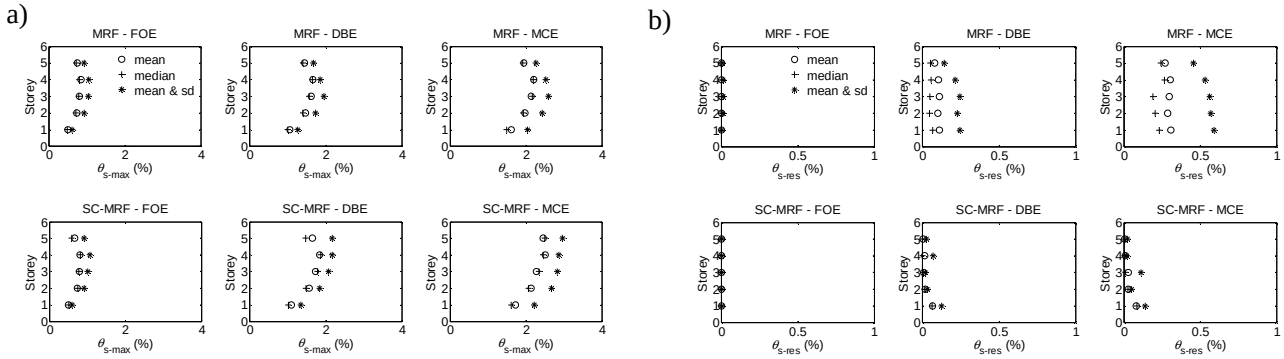

Figure 5 (a) Statistics of peak storey drifts of the conventional MRF and the SC-MRF under 20 earthquake ground motions scaled to the FOE, DBE and MCE; (b) Statistics of residual storey drifts of the conventional MRF and the SC-MRF under 20 earthquake ground motions scaled to the FOE, DBE and MCE

7 CONCLUSIONS

- The proposed model for the PT connection with WHPs and the associated beams and columns has been calibrated against experimental results and found to accurately simulate the hysteretic behaviour of the PT connection.
- Nonlinear static monotonic (pushover) analysis shows that the conventional MRF and the SC-MRF have comparable base shear strength and initial stiffness. The conventional MRF experiences significant damage in beams at the DBE drift. On the other hand, the SC-MRF has damage-free beams for drifts even higher than the MCE drift. Nonlinear static cyclic (push-pull) analysis shows that the SC-MRF has full re-centering capability and adequate energy dissipation capacity under the DBE.
- Seismic analyses show that for both MRF and SC-MRF the mean peak storey drifts are close to the design values. But the SC-MRF practically eliminates residual storey drifts apart from the first storey. On the other hand residual storey drifts of the MRF indicate that repair of damage in the conventional MRF would be costly and disruptive after the DBE and not financially viable after the MCE.

REFERENCES

Charney F.A., Downs W.M. (2004), Connections in steel structures V. ESSC/AISC Workshop, Amsterdam, June 3-4.

Dimopoulos A.I., Karavasilis T.L., Vasdravellis G., Uy B. (2013). Seismic design, modelling and assessment of self-centering steel frames using post-tensioned connections with web hourglass pins, *Bulletin of Earthquake Engineering*, DOI: 10.1007/s10518-013-9437-4

EC8. Eurocode 8 (2004), Design of structures for earthquake resistance.

EC3. Eurocode 3 (2003), Design of steel structures.

Kobori T., Miura Y., Fukuzawa E., Yamada T., Arita T., Takenaka Y., Miyagawa N., Tanaka N., Fukumoto T. (1992), *Development and application of hysteresis steel dampers*, Earthquake Engineering, Tenth World Conference. Rotterdam, Balkema.

Mazzoni S., McKenna F., Scott M., Fenves G. (2006), Open system for earthquake engineering simulation (OpenSees). *User Command Language Manual, Pacific Earthquake Engineering Research Center*, University of California, Berkeley.

Mc Cormick J., Aburano H., Ikenaga M., Nakashima M. (2008), *Permissible residual deformation levels for building structures considering both safety and human elements*, 14th WCEE, Beijing, China.

Vasdravellis G., Karavasilis T.L., Uy B. (2012), Large-scale experimental validation of steel post-tensioned connections with web hourglass pins, *Journal of Structural Engineering*, in press.

Vasdravellis G., Karavasilis T.L., Uy B. (2013). Finite element models and cyclic behaviour of self-centering steel post-tensioned connections with web hourglass pins, *Engineering Structures*, in press.